Published in final edited form as:
Neuroimage. 2011 June 1; 56(3): 1145–1153. doi:10.1016/j.neuroimage.2011.02.082.

White matter cerebral blood flow is inversely correlated with structural and functional connectivity in the human brain

Sina Aslan[a,b], **Hao Huang**[a,b], **Jinsoo Uh**[a], **Virendra Mishra**[a,b], **Guanghua Xiao**[c], **Matthias J.P. van Osch**[d], and **Hanzhang Lu**[a,b]

[a]Advanced Imaging Research Center, University of Texas Southwestern Medical Center, Dallas, TX 75390, United States [b]Biomedical Engineering Graduate Program, University of Texas Southwestern Medical Center, Dallas, TX 75390, United States [c]Division of Biostatistics, Department of Clinical Sciences, University of Texas Southwestern Medical Center, Dallas, TX 75390, United States [d]Department of Radiology, Leiden University Medical Center, Leiden, The Netherlands

Abstract

White matter provides anatomic connections among brain regions and has received increasing attention in understanding brain intrinsic networks and neurological disorders. Despite significant progresses made in characterizing the white matter's structural properties using post-mortem techniques and in vivo diffusion-tensor-imaging (DTI) methods, its physiology remains poorly understood. In the present study, cerebral blood flow (CBF) of the white matter was investigated on a fiber-tract-specific basis using MRI (N=10, 25-33 years old). It was found that CBF in the white matter varied considerably, up to a factor of two between fiber groups. Furthermore, a paradoxically inverse correlation was observed between white matter CBF and structural and functional connectivities (P<0.001). Fiber tracts that had a higher CBF tended to have a lower fractional anisotropy in water diffusion, and the gray matter terminals connected to the tract also tended to have a lower temporal synchrony in resting-state BOLD signal fluctuation. These findings suggest a clear association between white matter perfusion and gray matter activity, but the nature of this relationship requires further investigations given that they are negatively, rather than positively, correlated.

Keywords

fractional anisotropy; resting state; magnetic resonance imaging; arterial spin labeling; diffusion tensor imaging

Introduction

White matter provides anatomic connections between spatially distinct cortical regions and allows efficient propagation of neural signals (Waxman et al., 1995). Recent neuroimaging

Corresponding Author: Hanzhang Lu, Ph.D., Advanced Imaging Research Center, UT Southwestern Medical Center, 5323 Harry Hines Blvd., Dallas, TX 75390, Hanzhang.Lu@UTSouthwestern.edu, Tel: 214-645-2761, Fax: 214-645-2744.

studies have provided evidences that temporal coherence of activities in different gray matter regions is dependent upon the microstructural organization of the white matter connecting them (Greicius et al., 2009; Honey et al., 2009; Skudlarski et al., 2008; van den Heuvel et al., 2008; van den Heuvel et al., 2009). White matter structural changes have also been implicated in neurological diseases that were previously thought to be primarily affecting cortical regions (Kantarci et al., 2001; Voineskos et al., 2010). Despite mounting evidence of the role of white matter in understanding brain function, relatively little is known about the physiology of the white matter (van Gelderen et al., 2008; van Osch et al., 2009). The present study aims to investigate blood supply to the white matter in the human brain and its relationship with gray matter activity.

Neuroanatomy studies have revealed that blood vessels that perfuse white matter are branches of intracortical arteries that penetrate the cortical ribbon and often travel in parallel with the axon's path (see Supplemental Figure S1 for an illustration). Previous neuroimaging studies have also demonstrated the presence of blood flow in the white matter, but have not studied its spatial distribution due to limited sensitivity, resolution and the lack of supporting techniques. White matter contains highly specialized fiber tracts. These fibers serve different functional purposes with some requiring long-distance and rapid signal propagation (e.g. corticospinal tract) and others requiring dense but shorter connections (e.g. tracts connecting association cortices) (Conturo et al., 1999; Mori et al., 1999). We therefore hypothesized that cerebral blood flow (CBF) in the white matter varies between fiber tracts and that the tract-specific CBF is correlated with the fiber's structural property. Furthermore, given previous findings that functional connectivity in the gray matter is supported by white matter structural connection (Greicius et al., 2009), we hypothesized that functional measures of the white matter, e.g. CBF, may have a strong relationship to gray matter connectivity.

In the present study, we performed an MRI study with multiple sub-modalities. A recently developed quantitative Arterial Spin Labeling (qASL) MRI was used to obtain maps of absolute CBF (Aslan et al., 2010). Diffusion tensor imaging (DTI) was used to delineate ten major fiber tracts in the brain. The resulting voxel masks served as the regions-of-interest (ROIs) and were applied to the CBF maps to calculate the tract-specific CBF in the white matter. Across fiber tracts, CBF showed a paradoxically inverse correlation with fractional anisotropy (FA) obtained from DTI. Functional connectivity MRI (fcMRI) was performed to allow the assessment of resting-state neural activity in the gray matter connected by each tract. An inverse correlation was again observed between tract-specific CBF and the functional connectivity.

Materials and Methods

Participants

Human subjects were recruited from local community via flyers posted in the University of Texas (UT) Southwestern Medical Center campus. The Health Insurance Portability and Accountability Act (HIPAA) compliant protocol was approved by the UT Southwestern Institutional Review Board and written informed consent was obtained. All participants underwent extensive screening and had no contraindications for MRI scanning (e.g. pacemaker, implanted metallic objects, claustrophobia), and were generally of good health, with no serious or unstable medical conditions such as neurological disease, brain injury, uncontrollable shaking, or history of brain tumor. The participants had a narrow age range (25-33 years old) and were considered a relatively young group of subjects, as aging may change the distribution of CBF in the brain (Lu et al., 2010). A total of 10 subjects were studied with a similar representation from men and women (6 males and 4 females).

Experiment

MRI investigations were performed on a 3 Tesla MR system (Philips Medical System, Best, The Netherlands). A body coil was used for radiofrequency (RF) transmission and an 8-channel head coil with parallel imaging capability was used for signal reception. Foam padding was used to stabilize the head to minimize motion. The imaging protocol consisted of five MR techniques: qASL, DTI, fcMRI, T2-weighted echo-planar-imaging (EPI), and T1-weighted anatomic scan. In the following paragraphs, the detailed parameters of each of these techniques are provided.

Our laboratory has recently developed a quantitative ASL method in which a Pseudo-Continuous ASL (PCASL) sequence was combined with a phase-contrast sequence to obtain voxel-by-voxel CBF estimation in units of ml blood per 100 g of tissue per min (ml/100g/min) (Aslan et al., 2010). The ASL technique used in the present study was based on this method with an exception. We used spin-echo EPI acquisition instead of the more widely used gradient-echo so that the ASL image characteristics match that of DTI, enabling a more precise image registration between DTI and ASL. The PCASL sequence parameters were: Field-Of-View (FOV) = 200×200 mm^2, matrix = 80×80, slice thickness = 2.5 mm, 42 axial slices acquired in two packages, no gap between slices, voxel size = 2.5×2.5×2.5 mm^3, labeling duration = 1650 ms, post-labeling delay = 1525 ms, TR/TE = 4296ms/27ms, SENSE factor 2.5, time interval between consecutive slice acquisitions = 54.2 ms, number of controls/labels = 90 pairs, labeling RF pulse duration = 0.5 ms, pause between RF pulses = 0.5 ms, labeling pulse flip angle = 18°, and scan duration of 18 min. The phase-contrast MRI was performed to provide a calibration factor for CBF quantification (Aslan et al., 2010) and used the following sequence parameters: slice location = perpendicular to the four major feeding arteries (left/right internal carotid and vertebral arteries) at the level of cervical spine 3 (C3), FOV = 230×230 mm^2, voxel size = 0.45×0.45×5 mm^3, TR/TE/flip angle=20ms/7ms/15°, encoding velocity = 80 cm/s, and scan duration = 1.5 minutes. The subject was instructed to fixate on a white cross-hair during the ASL scan to maintain their attention and wakefulness.

DTI provided an assessment of anatomic connections between brain regions and also delineated distinctive white matter structures through tractography (Mori et al., 1999). The DTI scan used relatively standard parameters and the spatial resolution was identical to that of ASL: single-shot spin-echo EPI, FOV = 200×200 mm^2, matrix = 80×80, slice thickness = 2.5 mm, no gap between slices, voxel size = 2.5×2.5×2.5 mm^3, 58 slices, SENSE factor 2.5, TR/TE=5025ms/59ms. 30 gradient-encoding directions with a *b* value of 1000 s/mm^2, scan duration 3 minutes.

FcMRI used temporal correlations between gray matter MR signal time courses to assess functional connectivity of the brain at rest (Biswal et al., 1995; Raichle et al., 2001). The subject fixated on a cross-hair while Blood-Oxygenation-Level-Dependent (BOLD) images were acquired. The sequence parameters were: FOV = 200×200, matrix = 80×80, slice thickness = 5 mm, no gap between slices, voxel size=2.5×2.5×5 mm^2, 29 axial slices, TR/TE/flip angle=1500ms/30ms/60°, 400 image volumes, scan duration = 10 minutes. The in-plane resolution of the fcMRI scan was identical to that of ASL and DTI, but the slice thickness was greater to ensure a sufficient signal-to-noise ratio (SNR). In addition, fcMRI used gradient-echo acquisition rather than spin-echo to maximize the BOLD contrast.

In addition to the three main techniques described above, two other scans were performed. A T2-weighted EPI image was acquired immediately before the PCASL scan to serve as a template to which all other images were coregistered. The sequence parameters were: single-shot spin-echo EPI, FOV = 200×200 mm^2, matrix = 80×80, slice thickness = 2.5 mm, no gap between slices, voxel size = 2.5×2.5×2.5 mm^3, 58 slices, SENSE factor 2.5, TR/TE/flip

angle=5000ms/59ms/90°, four averages, duration = 20 seconds. The T2-weighted image had the same contrast as the *b0* image in DTI, making it straightforward to coregister between these images. The image contrast of PCASL was slightly different from the T2 weighted image due to the shorter TE (i.e. more proton-density weighted), but the time gap between the two scans was less than 20 seconds (i.e. the preparation time of PCASL sequence) thus we expected minimal motion between these two images. In addition, a high-resolution T1-weighted image was acquired for anatomic reference and for the estimation of brain volume. The sequence parameters were: Magnetization-Prepared-Rapid-Acquisition-of-Gradient-Echo (MPRAGE) sequence, TR/TE/flip angle = 8.3ms/3.8ms/12°, 160 sagittal slices, voxel size = 1×1×1 mm^3, FOV = 256×256×160 mm^3, and scan duration 4 min.

Data Pre-processing

PCASL image series were realigned to the first volume for motion correction (SPM2's realign function, University College London, UK). Similarly, the images in fcMRI were realigned to its first volume. The images in T2 EPI were realigned to the last volume because it was the closest to the PCASL scan. The DTI image series were coregistered to the *b0* image using an affine transformation (SPM2's coregistration function). After these intra-scan registrations, inter-scan registrations were conducted. The mean image in T2 EPI was used as a template and the spatial transformation matrix between the other images and the template was computed. Figure 1 shows a demonstration of image coregistration schemes and representative parametric maps (e.g. FA, CBF, and white matter probability).

The labeled images in PCASL were subtracted from the control images and, after calibration using the phase-contrast data (Aslan et al., 2010), CBF maps in units of ml/100g/min were calculated (Matlab, Mathworks, Natick, MA). The CBF maps were then registered to the template space using the transformation matrix computed earlier. DTI data were processed using the software DTIStudio (The Johns Hopkins University, Baltimore, MD) to obtain standard parametric maps of FA, apparent diffusion coefficient (ADC), and radial/axial diffusivities. Fiber-tracking was performed on the DTI data. To avoid potential controversies on the validity of the small fibers, the tract-specific CBF investigation was limited to ten major fiber tracts that have been previously shown to be highly reproducible across raters and across data sets (Wakana et al., 2007): forceps major of the corpus callosum, forceps minor of the corpus callosum, cingulum in the cingulate cortex, cingulum to hippocampus, anterior thalamic radiation, uncinate fasciculus, corticospinal tract, arcuate fasciculus, inferior fronto-occipital fasciculus, and inferior longitudinal fasciculus. The masks of the fiber tracts as well as the FA and ADC maps were transformed to the T2 EPI template space. The T2 EPI image was segmented using SPM2's segmentation function to yield probability maps of white matter, gray matter and CSF. Unless otherwise specified, all further image computation was carried out in the template space.

Data Post-processing

Tract-specific CBF was obtained by applying the DTI tract mask to the CBF map. To ensure that our ROI included predominantly white matter and to minimize gray matter partial volume effect, two procedures were undertaken. First, only voxels that had white matter probability of >50% were included in the final ROI. Second, the resulting spatially averaged CBF value was further divided by a correction factor, $P_{wm}+2.5\times P_{gm}$, where the gray/white matter CBF ratio was assumed to be 2.5. This strategy has previously shown to be useful in correcting for gray/white matter partial volume in CBF data (Lu et al., 2005). Tract-specific FA and ADC values were also obtained by averaging voxels in the final ROI.

Signal-to-noise ratio (SNR) of CBF in each fiber tract was computed from the PCASL data. The voxels in the fiber tract was averaged to obtain a CBF time course of 90 points. The

signal level was calculated as the mean of the time course and the noise level as the standard error (i.e. standard deviation divided by $\sqrt{90}$) (Aslan and Lu, 2010).

The fcMRI data provided an assessment of functional connectivity between two gray matter regions that were connected by a specific fiber tract. In the present study, we defined the fcMRI ROIs based on the white matter tract, in order to compare the correspondence between gray matter connectivity and white matter CBF. In the DTI space, the fiber terminals of each end of each tract were identified. Then, the mask containing the terminals was expanded spherically by three voxels (7.5 mm in radius) using an Interactive Data Language (IDL) program. A three-voxel expansion was chosen to make certain that the entire cortical ribbon connected to the tract was included. The expanded mask was then transformed to the T2 EPI template space. To ensure that only gray matter voxels were included in the fcMRI analysis, the mask was thresholded at gray matter probability of greater than 50% to yield the final fcMRI ROI. The corticospinal tract was excluded from this analysis because the terminal of this tract was in the spinal cord which was beyond the spatial coverage of our image acquisition.

Cross-correlation coefficient (cc) between the time courses from the two fcMRI ROIs was computed. The conventional approach to compare cc values across connections was to average the time courses of all voxels in each ROI and to calculate cc. However, different tracts have different sizes, and thus the associated gray matter ROIs were also different in their volume. This would result in different SNR for different tracts, which may affect the comparison of cc values across tracts. Therefore, to minimize the effect of SNR on the estimation of cc, we calculated the cc values using a modified approach. We first divided each ROI into “blocks” of ten voxels. For example, if the two terminals of a tract had 300 and 400 voxels, respectively, then they would have 30 and 40 blocks, respectively. The cc value between each possible pair of blocks can be calculated, yielding a total of 1,200 cc values. These cc values were converted to z-scores by a Fisher transform, followed by averaging and transforming back to cc by an inverse Fisher transform. The grouping of the voxels into blocks was performed by random assignment via a Matlab script. The random assignment was repeated 100 times and the averaged cc value was used in the statistical analysis.

Assessment of white matter probability and layer index

Since gray and white matters are known to have different CBF values, potential partial voluming of gray matter in our fiber tract ROI may affect the estimation of white matter CBF. The variance in the extent of partial voluming across tracts may even cause a false-positive correlation between CBF and FA. Therefore, we computed the white matter probability for each tract using the probability map segmented from the T2 EPI image. The fiber’s white matter probability was used as a covariate in the correlation analyses (detailed below).

Given that arteries perfusing the white matter are branches originating from the cortical surface (Duvernoy et al., 1981), it is possible that white matter CBF could also be dependent on the location, with tissues close to the cortex having higher CBF and tissue deep in the brain having lower CBF (i.e. watershed effect). This is especially relevant for ASL-derived CBF in which the arterial transit time may increase from superficial to deep white matter and may affect the CBF measurement (Alsop and Detre, 1996). We therefore estimated a “layer index” for each voxel in the white matter. We used a stepwise erosion method in which each step consisted of “peeling off” one layer of voxels from the white matter mask and then assigned one layer index. Continuing this process resulted in a gradually decreasing white matter volume with increasing layer indices (see Supplemental Figure S2 for an

example of layer index map). With this procedure, each voxel was assigned a layer index and the fiber tract's layer index was calculated by averaging the indices of the voxels. The white matter layer index of the tract was used as a covariate in the correlation analyses.

Statistical Analysis

We compared white matter CBF across fiber tracts using a one-way Analysis-of-Variance (ANOVA). Post-hoc Tukey's honest significance tests were conducted for pair-wise comparisons.

Correlations between white matter CBF and FA across fiber tracts were assessed using a meta-analysis method (Miller, 1981). Briefly, Pearson correlation coefficients between CBF and FA were calculated for each subject. The cc values were then converted to z-scores using a Fisher transform. A one-sample t test was then performed on the z-scores to determine whether they were significantly different from zero. To account for potential confounding effects from partial volume and/or white matter arterial transit time, the meta-analysis approach described above was repeated using partial correlation (using matlab function partialcorr.m) between CBF and FA, after factoring out the contributions from white matter probability and layer index. The use of partial correlations was helpful for controlling for other factors (e.g. partial voluming) that may have influenced the correlation between CBF and FA, and has been widely used in previous neuroimaging studies (Achard et al., 2006; Liu et al., 2008; Salvador et al., 2005; van den Heuvel et al., 2008). A relationship was considered significant only if both the Pearson correlation and the partial correlation had a multiple-comparison-corrected P value of 0.05 or less.

Similar meta-analyses were performed for correlations comparing CBF to radial diffusivity, axial diffusivity, ADC, and fcMRI cc. We also studied correlations between FA and fcMRI cc.

Correlation coefficients between the tract-specific CBF, white matter probability, and layer index were calculated and one-sample t tests were performed.

In addition to the ROI analysis, a voxel-based spatial correlation was assessed for white matter CBF and FA. For each voxel in the white matter (probability>50%), a CBF and FA can be obtained. Thus the data from all white matter voxels in the brain can yield an array of CBF and an array of FA. The Pearson correlation between these arrays was calculated for each subject, which was converted to a z-score using Fisher transform and was subject to a one-sample t test. The analysis was then repeated using partial correlations (i.e. after factoring out the voxel-by-voxel white matter probability and layer index values). Again, the relationship was considered significant only if both the Pearson correlation and the partial correlation had a P value of 0.05 or less.

Results

Figures 2a and b show the locations of the major fiber tracts in a representative subject. Table 1 summarizes the tract-specific CBF, FA, white matter probability, layer index, SNR of tract-specific CBF as well as the fcMRI cc values from the gray matters that the respective tract connects. Note that the white matter probabilities of the fiber tracts were all above 90%, which suggest that 1) the calculated CBF was largely from the white matter voxels and 2) the coregistration between image sub-modalities was effective because the tract masks were delineated from DTI data while the probability maps were computed from T2 EPI data. The average CBF values of all white matter tracts were 16.1±3.1 mL/100g/min. Significant differences in CBF were observed across fiber tracts (ANOVA, omnibus F test, $P<0.001$). Results of post-hoc pairwise comparison between tracts showed that the CBF was

highly heterogeneous and a significant difference was detected in many of the comparisons (after multi-comparison corrections) (Supplemental Table S1).

Figure 2c shows the scatter plots between CBF and FA for individual subjects. An inverse correlation is observed in each subject. That is, a fiber tract that had a higher FA value tended to have a lower CBF, and vice versa. Using data from all subjects, meta-analysis showed a significant correlation between these two parameters (partial $r=-0.66\pm0.18$, multiple-comparison-corrected $P<0.001$). We also investigated whether the correlation with FA is associated with radial or axial diffusivity or both. It was observed that CBF was positively correlated with radial diffusivity (partial $r=0.46\pm0.22$, multiple-comparison-corrected $P=0.001$) and negatively correlated with axial diffusivity (partial $r=-0.60\pm0.32$, $P=0.003$), suggesting that both of these diffusion components contributed to the FA correlation. Figure 3 shows the scatter plot between CBF and radial and axial diffusivity for the group-averaged data. Tract-specific CBF was also found to be inversely correlated with ADC values (partial $r=-0.53\pm0.16$, $P<0.001$) (Figure 3c). The tract-based results were confirmed by voxel-based results. Spatial partial correlation coefficient between CBF and FA maps was found to be -0.19 ± 0.02 (mean±std, N=10) (Supplemental Figure S3) and was statistically significant ($P<0.001$).

Figure 4a shows the gray matter nodes (green) obtained from an expansion of white matter (red) terminals using “cingulum-in-the-cingulated-cortex” tract as an example. The results for other tracts were similar. Figure 4b shows the scatter plots between CBF and fcMRI cc across fiber tracts, listed for each subject. An inverse correlation was observed in each subject. That is, a fiber tract that had a higher CBF value tended to have a lower cc between the two terminal gray matter regions connected by this tract, and vice versa. Using data from all subjects, meta-analysis showed a significant correlation between these two parameters (partial $r=-0.52\pm0.20$, multiple-comparison-corrected $P<0.001$). Comparing FA and fcMRI cc values, a positive correlation was observed (partial $r=0.76\pm0.09$, $P<0.001$). Figure 5 shows the scatter plot between FA and cc for the group-averaged data. The ADC values of the fiber tracts were not correlated with the fcMRI cc ($P=0.74$). Potential relationship between gray matter CBF and fcMRI cc was also assessed. There was not a statistically significant correlation between these parameters.

Tract-specific CBF was also compared to white matter probability. A trend toward an inverse relationship was observed (multiple-comparison-corrected $P=0.114$) (see Supplemental Figure S4 for a scatter plot), but the level of significance was much lower compared to FA or fcMRI.

Erosion analysis revealed that white matter CBF gradually decreased from superficial layers to deep layers (Supplemental Figure S5). However, this effect could not explain the differences in CBF across fiber tracts because the layer index was not correlated with tract-specific CBF (uncorrected $P=0.266$) (see Supplemental Figure S6 for a scatter plot).

Discussion

The present study provided a quantitative assessment of blood supply in the white matter. It was found that CBF in the white matter was distributed heterogeneously and variation in CBF across fiber tracts can be more than a factor of two. Furthermore, a strong correlation was observed between white matter CBF and structural and functional connectivities as measured by MRI techniques. Fiber tracts that had a higher CBF tended to have a lower fractional anisotropy in water diffusion, and the gray matter terminals connected to the tract also tended to have a lower temporal synchrony in resting-state BOLD signal fluctuation.

In recent years, there has been a growing interest to understand functional connectivity among distinctive brain regions (Biswal et al., 1995; Greicius et al., 2009; Honey et al., 2009; Raichle et al., 2001; van den Heuvel et al., 2009). Some evidence has suggested that such a functional connectivity is supported by structural connection via white matter fiber tracts (Greicius et al., 2009; Honey et al., 2009; van den Heuvel et al., 2008). It can be further hypothesized that functional measures of the white matter, e.g. perfusion, may have a more direct link to gray matter connectivity, compared to simple structural measures. Our study indeed confirmed the presence of a significant relationship between white matter CBF and the degree of gray matter functional connectivity. The sign of correlation was, however, negative, whereas the most intuitive expectation would have been a positive correlation based on the presumption that fiber tracts providing a “stronger” connection would be metabolically more active, thereby requiring higher CBF. These findings suggest that the mechanism of the association may not be the neurovascular coupling that governs the perfusion in the gray matter. This is possibly because in the white matter there is little neurotransmitter release or astrocyte signaling that is thought to mediate the blood flow response in the gray matter (Attwell and Iadecola, 2002; Zonta et al., 2003). This observation also supports the notion that CBF is not coupled to action potentials (Logothetis et al., 2001; Mathiesen et al., 1998).

To our knowledge, the present study is the first report of a tract-based CBF with an inverse correlation between CBF, FA, and fcMRI cc values. In addition, FA was found to be positively correlated with fcMRI cc value, which confirms a recent report by van den Heuvel et al. (2008). The relationship between FA and fcMRI cc can also be readily predicted from the observations that both are inversely correlated with CBF. Although this report has focused on comparisons across fiber tracts, we have also tested the correlations across subjects and found a similar inverse relationship between white matter CBF and FA (partial $r=-0.50\pm0.26$, multiple-comparison-corrected $P=0.001$).

We propose three possible mechanisms that may be responsible for the observed inverse correlations: 1) white matter CBF may be related to averaged axonal diameter of the tract; 2) lower white matter CBF may reflect a higher efficiency of action potential propagation; 3) white matter CBF may be affected by the mechanical tightness of the fiber bundle. Our results show that CBF is negatively correlated with FA and axial diffusivity, but is positively correlated with radial diffusivity. Similar relationships with these DTI parameters have recently been reported for the axonal diameters. Barazany et al. showed that the mean axonal diameter determined using an AxCaliber technique is negatively correlated with FA and axial diffusivity, but is positively correlated with radial diffusivity (Barazany et al., 2009). Using a different technique called orientationally invariant indices to estimate axonal diameter, Alexander and colleagues demonstrated the same relationships (Alexander et al., 2010). The similarity between these reports and findings in the present study leads to the hypothesis that CBF in white matter tracts may be associated with the axonal diameter. Axons of greater caliber tend to have a larger capacitance and may require more ion flux to achieve depolarization and repolarization, which necessitates more activities of Na^+/K^+-ATPase pumps and a greater blood supply. Indeed, some neuroanatomy literature suggests that forceps minor and major which are located in the genu and splenium of the corpus callosum, respectively, and manifest lower CBF in our data, have a relatively small mean axonal diameter of 0.5-1.0 microns (Aboitiz et al., 1992; Lamantia and Rakic, 1990); corticospinal tract which receives a larger CBF has a mean diameter of 1.2-2 microns (Biedenbach et al., 1986; Deschenes and Landry, 1980); the thalamic-cortical tract which shows an even greater CBF has an axonal diameter of 2-3 microns (Deschenes and Landry, 1980). In addition, for a given voxel size, larger axons would correspond to a lower axonal density (Alexander et al., 2010). Thus there are fewer fibers to connect between the terminal

gray matter regions, which may be responsible for the lower signal synchrony in the fcMRI data.

There are other possible mechanisms for the observed relationships. FA is thought to increase with myelin sheath (Avram et al., 2010; Song et al., 2002b), which restricts the water motion in the cross-sectional direction thereby increasing the anisotropy of water diffusion. Electrophysiologically, myelin sheath acts as an insulator and increases the propagation efficiency of electrical signals in the axon so that Na^+/K^+-ATPase pumps are only needed at discrete points called Nodes of Ranvier (Waxman et al., 1995). As such, the energy demand may be inversely correlated with myelin sheath and its density, thus blood supply is also inversely correlated with FA. Another possible mechanism is that the relationship may simply reflect differential mechanical properties across fiber tracts. That is, tracts that are tightly packed may be more difficult for the blood to perfuse due to the need to counteract a greater pressure, whereas those that are more loosely structured may receive more blood flow. Interestingly, this notion is consistent with recent literature that white matter CBF in older subjects was found to be higher than that in younger subjects (Lu et al., 2010), possibly because white matter in elderly is microstructurally less dense and shows a lower FA (Salat et al., 2005). We also note that the possible explanations above are not necessarily incompatible to each other. For example, voxels containing smaller caliber axon tend to have a relatively larger fraction of myelin and may be easier to be packed densely.

In evaluating the validity of our results, we have paid special attention to partial voluming effects to rule out the possibility that this observation was due to confounding factors. We applied a threshold (50%) on white matter probability so that only voxels higher than the threshold were included in the parametric assessment. As a result, the white matter probability in the final tract ROIs was above 90% for all cases (Table 1). In addition, we divided the averaged CBF values by $P_{wm}+2.5\times P_{gm}$ to further correct for the residual gray matter partial volume (Lu et al., 2005). Moreover, in the correlation analyses between CBF and other parameters, white matter probability was included as a covariate (Liu et al., 2008). The results showed that the inverse correlation was still present after the inclusion of the covariate. We have also considered the possible effect of the vascular anatomy on white matter CBF. The arterial vessels in the white matter typically originate from the brain surface and penetrate through the cortical ribbon to enter the white matter (Supplemental Figure S1). Therefore, it may take more time for the blood to reach the deep white matter compared to the superficial white matter. The ASL signal of deep white matter may then be under-estimated due to greater T1 relaxation and, despite the addition of post-labeling delay to reduce the sensitivity to timing (Alsop and Detre, 1996;Luh et al., 1999), it may still be affected by the arterial transit time. Therefore, we used an image erosion method to obtain a layer index (Layer 1 indicated the outermost layer, Supplemental Figure S2) for each voxel and tract, and included this index as a covariate in all correlation analyses. Our results showed that the inverse correlations were still present after factoring out the effect of layer index. To further confirm the inverse correlation observed in the tract-based analysis, we conducted a voxel-by-voxel spatial correlation analysis and the results again showed a significant negative correlation. Therefore, the results from the different analysis approaches seem to suggest a consistent negative correlation between white CBF and FA. This relationship is further collaborated by the negative correlation between CBF and fcMRI cc values. Note that the CBF and fcMRI cc were obtained from mutually exclusive ROIs (i.e. CBF from white matter, fcMRI from gray matter), thus partial volume effect in the fiber tracts could not possibly cause such a finding. We have also considered the possibility that CBF may influence the estimation of FA. Voxels in the white matter contain both tissue and vasculature. Although tissue (including axon and myelin) is often the primary focus in FA considerations, a small amount of blood (about 1.4%) (Lu et al., 2005) is also present in the white matter and may affect the FA value estimated from our DTI sequence. The signal

attenuation of the blood signal with field gradient is often more rapid because of the intravoxel incoherent motion (IVIM) mechanism (Le Bihan et al., 1986;Song et al., 2002a), and is isotropic along all directions. This partial voluming may cause a CBF-dependent under-estimation in FA. We have conducted a simulation in which the tissue FA was assumed to be fixed at 0.50 and the CBF was varied from 10-20 ml/100g/min. The CBV was varied with CBF according to Grubb's equation (Grubb et al., 1974). We found that, although CBF had an influence on the estimated FA, the size of the effect was very small. Within the CBF range simulated, the FA only changed by 0.002, which is almost two orders less than the observed FA variations. This could also be tested experimentally using blood nulling or mild diffusion weighting in future studies.

The findings from the present study should be interpreted in view of a few limitations. First, our analysis has primarily focused on ten major white matter tracts, but has not investigated other smaller fibers. These ten tracts were selected because they were previously shown to be highly reproducible across subjects and raters (Wakana et al., 2007). However, whether the findings are extendable to other white matter requires further investigation. Second, the SNR of ASL in the white matter is known to be relatively poor (van Gelderen et al., 2008). Despite recent advances in ASL technologies (van Osch et al., 2009) and our efforts to increase the sensitivity by using a long scan duration (18 min), the SNR in the present study was still in a low range of 4.4-14.6. Therefore, our findings need to be replicated by future studies with improved methodology (e.g. ASL at 7 Tesla). Third, the potential confounding factor of arterial arrival time was assessed by including a layer index as a covariate in the correlation analysis. An implicit assumption in using this approach was that the arrival time was presumed to be solely dependent on the depth of the voxel (i.e. the deeper, the longer). The actual arrival time, however, may be also dependent on the perfusion territory of feeding arteries (Hendrikse et al., 2008; van Laar et al., 2006). Cerebral border zones may have excessively long arrival time, which may result in smaller apparent ASL signals. In future work, an arrival time map should be acquired and used as a covariate in place of the lay index. Finally, the present study has only included young, healthy subjects. Whether the observed relationship will be applicable for older group and patient populations requires further investigation.

Conclusions

We found that blood flow in the white matter is inversely correlated with the anisotropy of water diffusion as well as the gray matter's temporal synchrony. These data suggest that perfusion in the white matter is strongly associated with gray matter's connectivity, but its mechanism may be related to microstructural organization of the fiber tract rather than the neurovascular coupling phenomenon that governs the relationship between neural activity and hemodynamics in the gray matter.

Supplementary Material

Refer to Web version on PubMed Central for supplementary material.

Acknowledgments

The authors are grateful to Nyaz Didehbani for scientific editing of the manuscript. We also thank two anonymous reviewers for helpful suggestions. This study was supported in part by NIH grants R01 MH084021 (to HL), NIH R01 NS067015 (to HL), NIH R21 EB007821 (to HL), American Heart Association 0865003F (to HL).

References

Aboitiz F, Scheibel AB, Fisher RS, Zaidel E. Fiber composition of the human corpus callosum. Brain Res. 1992; 598:143–153. [PubMed: 1486477]

Achard S, Salvador R, Whitcher B, Suckling J, Bullmore E. A resilient, low-frequency, small-world human brain functional network with highly connected association cortical hubs. J Neurosci. 2006; 26:63–72. [PubMed: 16399673]

Alexander DC, Hubbard PL, Hall MG, Moore EA, Ptito M, Parker GJ, Dyrby TB. Orientationally invariant indices of axon diameter and density from diffusion MRI. Neuroimage. 2010; 52:1374–1389. [PubMed: 20580932]

Alsop DC, Detre JA. Reduced transit-time sensitivity in noninvasive magnetic resonance imaging of human cerebral blood flow. J Cereb Blood Flow Metab. 1996; 16:1236–1249. [PubMed: 8898697]

Aslan S, Lu H. On the sensitivity of ASL MRI in detecting regional differences in cerebral blood flow. Magn Reson Imaging. 2010; 28:928–935. [PubMed: 20423754]

Aslan S, Xu F, Wang PL, Uh J, Yezhuvath US, van Osch M, Lu H. Estimation of labeling efficiency in pseudocontinuous arterial spin labeling. Magn Reson Med. 2010; 63:765–771. [PubMed: 20187183]

Attwell D, Iadecola C. The neural basis of functional brain imaging signals. Trends Neurosci. 2002; 25:621–625. [PubMed: 12446129]

Avram AV, Guidon A, Song AW. Myelin water weighted diffusion tensor imaging. Neuroimage. 2010; 53:132–138. [PubMed: 20587369]

Barazany D, Basser PJ, Assaf Y. In vivo measurement of axon diameter distribution in the corpus callosum of rat brain. Brain. 2009; 132:1210–1220. [PubMed: 19403788]

Biedenbach MA, De Vito JL, Brown AC. Pyramidal tract of the cat: axon size and morphology. Exp Brain Res. 1986; 61:303–310. [PubMed: 3948941]

Biswal B, Yetkin FZ, Haughton VM, Hyde JS. Functional connectivity in the motor cortex of resting human brain using echo-planar MRI. Magn Reson Med. 1995; 34:537–541. [PubMed: 8524021]

Conturo TE, Lori NF, Cull TS, Akbudak E, Snyder AZ, Shimony JS, McKinstry RC, Burton H, Raichle ME. Tracking neuronal fiber pathways in the living human brain. Proc Natl Acad Sci U S A. 1999; 96:10422–10427. [PubMed: 10468624]

Deschenes M, Landry P. Axonal branch diameter and spacing of nodes in the terminal arborization of identified thalamic and cortical neurons. Brain Res. 1980; 191:538–544. [PubMed: 7378769]

Duvernoy HM, Delon S, Vannson JL. Cortical blood vessels of the human brain. Brain Res Bull. 1981; 7:519–579. [PubMed: 7317796]

Greicius MD, Supekar K, Menon V, Dougherty RF. Resting-state functional connectivity reflects structural connectivity in the default mode network. Cereb Cortex. 2009; 19:72–78. [PubMed: 18403396]

Grubb RL Jr. Raichle ME, Eichling JO, Ter-Pogossian MM. The effects of changes in PaCO2 on cerebral blood volume, blood flow, and vascular mean transit time. Stroke. 1974; 5:630–639. [PubMed: 4472361]

Hendrikse J, Petersen ET, van Laar PJ, Golay X. Cerebral border zones between distal end branches of intracranial arteries: MR imaging. Radiology. 2008; 246:572–580. [PubMed: 18055872]

Honey CJ, Sporns O, Cammoun L, Gigandet X, Thiran JP, Meuli R, Hagmann P. Predicting human resting-state functional connectivity from structural connectivity. Proc Natl Acad Sci U S A. 2009; 106:2035–2040. [PubMed: 19188601]

Kantarci K, Jack CR Jr. Xu YC, Campeau NG, O'Brien PC, Smith GE, Ivnik RJ, Boeve BF, Kokmen E, Tangalos EG, Petersen RC. Mild cognitive impairment and Alzheimer disease: regional diffusivity of water. Radiology. 2001; 219:101–107. [PubMed: 11274543]

Lamantia AS, Rakic P. Cytological and quantitative characteristics of four cerebral commissures in the rhesus monkey. J Comp Neurol. 1990; 291:520–537. [PubMed: 2329189]

Le Bihan D, Breton E, Lallemand D, Grenier P, Cabanis E, Laval-Jeantet M. MR imaging of intravoxel incoherent motions: application to diffusion and perfusion in neurologic disorders. Radiology. 1986; 161:401–407. [PubMed: 3763909]

Liu Y, Liang M, Zhou Y, He Y, Hao Y, Song M, Yu C, Liu H, Liu Z, Jiang T. Disrupted small-world networks in schizophrenia. Brain. 2008; 131:945–961. [PubMed: 18299296]

Logothetis NK, Pauls J, Augath M, Trinath T, Oeltermann A. Neurophysiological investigation of the basis of the fMRI signal. Nature. 2001; 412:150–157. [PubMed: 11449264]

Lu H, Law M, Johnson G, Ge Y, van Zijl PC, Helpern JA. Novel approach to the measurement of absolute cerebral blood volume using vascular-space-occupancy magnetic resonance imaging. Magn Reson Med. 2005; 54:1403–1411. [PubMed: 16254955]

Lu H, Xu F, Rodrigue KM, Kennedy KM, Cheng Y, Flicker B, Hebrank AC, Uh J, Park DC. Alterations in Cerebral Metabolic Rate and Blood Supply across the Adult Lifespan. Cereb Cortex. 2010 doi: 10.1093/cercor/bhq1224; In-press.

Luh WM, Wong EC, Bandettini PA, Hyde JS. QUIPSS II with thin-slice TI1 periodic saturation: a method for improving accuracy of quantitative perfusion imaging using pulsed arterial spin labeling. Magn Reson Med. 1999; 41:1246–1254. [PubMed: 10371458]

Mathiesen C, Caesar K, Akgoren N, Lauritzen M. Modification of activity-dependent increases of cerebral blood flow by excitatory synaptic activity and spikes in rat cerebellar cortex. J Physiol. 1998; 512(Pt 2):555–566. [PubMed: 9763643]

Miller, RG. Simultaneous Statistical Inference. Springer Publishing Company; New York, NY: 1981.

Mori S, Crain BJ, Chacko VP, van Zijl PC. Three-dimensional tracking of axonal projections in the brain by magnetic resonance imaging. Ann Neurol. 1999; 45:265–269. [PubMed: 9989633]

Raichle ME, MacLeod AM, Snyder AZ, Powers WJ, Gusnard DA, Shulman GL. A default mode of brain function. Proc Natl Acad Sci U S A. 2001; 98:676–682. [PubMed: 11209064]

Salat DH, Tuch DS, Greve DN, van der Kouwe AJ, Hevelone ND, Zaleta AK, Rosen BR, Fischl B, Corkin S, Rosas HD, Dale AM. Age-related alterations in white matter microstructure measured by diffusion tensor imaging. Neurobiol Aging. 2005; 26:1215–1227. [PubMed: 15917106]

Salvador R, Suckling J, Coleman MR, Pickard JD, Menon D, Bullmore E. Neurophysiological architecture of functional magnetic resonance images of human brain. Cereb Cortex. 2005; 15:1332–1342. [PubMed: 15635061]

Skudlarski P, Jagannathan K, Calhoun VD, Hampson M, Skudlarska BA, Pearlson G. Measuring brain connectivity: diffusion tensor imaging validates resting state temporal correlations. Neuroimage. 2008; 43:554–561. [PubMed: 18771736]

Song AW, Woldorff MG, Gangstead S, Mangun GR, McCarthy G. Enhanced spatial localization of neuronal activation using simultaneous apparent-diffusion-coefficient and blood-oxygenation functional magnetic resonance imaging. Neuroimage. 2002a; 17:742–750. [PubMed: 12377149]

Song SK, Sun SW, Ramsbottom MJ, Chang C, Russell J, Cross AH. Dysmyelination revealed through MRI as increased radial (but unchanged axial) diffusion of water. Neuroimage. 2002b; 17:1429–1436. [PubMed: 12414282]

van den Heuvel M, Mandl R, Luigjes J, Hulshoff Pol H. Microstructural organization of the cingulum tract and the level of default mode functional connectivity. J Neurosci. 2008; 28:10844–10851. [PubMed: 18945892]

van den Heuvel MP, Mandl RC, Kahn RS, Hulshoff Pol HE. Functionally linked resting-state networks reflect the underlying structural connectivity architecture of the human brain. Hum Brain Mapp. 2009; 30:3127–3141. [PubMed: 19235882]

van Gelderen P, de Zwart JA, Duyn JH. Pittfalls of MRI measurement of white matter perfusion based on arterial spin labeling. Magn Reson Med. 2008; 59:788–795. [PubMed: 18383289]

van Laar PJ, Hendrikse J, Golay X, Lu H, van Osch MJ, van der Grond J. In vivo flow territory mapping of major brain feeding arteries. Neuroimage. 2006; 29:136–144. [PubMed: 16095923]

van Osch MJ, Teeuwisse WM, van Walderveen MA, Hendrikse J, Kies DA, van Buchem MA. Can arterial spin labeling detect white matter perfusion signal? Magn Reson Med. 2009; 62:165–173. [PubMed: 19365865]

Voineskos AN, Lobaugh NJ, Bouix S, Rajji TK, Miranda D, Kennedy JL, Mulsant BH, Pollock BG, Shenton ME. Diffusion tensor tractography findings in schizophrenia across the adult lifespan. Brain. 2010; 133:1494–1504. [PubMed: 20237131]

Wakana S, Caprihan A, Panzenboeck MM, Fallon JH, Perry M, Gollub RL, Hua K, Zhang J, Jiang H, Dubey P, Blitz A, van Zijl P, Mori S. Reproducibility of quantitative tractography methods applied to cerebral white matter. Neuroimage. 2007; 36:630–644. [PubMed: 17481925]

Waxman, SG.; Kocsis, JD.; Stys, PK. The axon: structure, function and pathophysiology. 1 ed.. Oxford University Press; New York, NY: 1995.

Zonta M, Angulo MC, Gobbo S, Rosengarten B, Hossmann KA, Pozzan T, Carmignoto G. Neuron-to-astrocyte signaling is central to the dynamic control of brain microcirculation. Nat Neurosci. 2003; 6:43–50. [PubMed: 12469126]

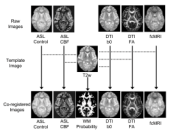

Figure 1.
Illustration of image coregistration procedures across modalities and examples of parametric maps. The T2-weighted (T2w) EPI image was used as a template to which all other images are coregistered. The T2w image was also used for segmentation of the brain into gray matter, white matter and CSF. The probability map of the white matter is shown.

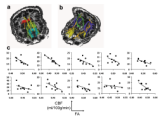

Figure 2.
Relationship between tract-specific FA and CBF. (a,b) Illustration of ten major fiber tracts overlaid on FA maps. For clarity, five fibers are shown in (a) and five are shown in (b). The fibers in (a) are: forceps major of the corpus callosum (red), forceps minor of the corpus callosum (blue), cingulum in the cingulate cortex (yellow), cingulum to hippocampus (orange), and anterior thalamic radiation (green). The fibers in (b) are: uncinate fasciculus (yellow), corticospinal tract (green), arcuate fasciculus (pink), inferior fronto-occipital fasciculus (blue), and inferior longitudinal fasciculus (orange). (c) Scatter plots between FA and CBF across fiber tracts. Each sub-plot displays data from one subject. Within a sub-plot, different points indicate different tracts. An inverse correlation is observed in all subjects. In statistical analysis, the cc values from the sub-plots are combined in a meta-analysis to yield a t statistic.

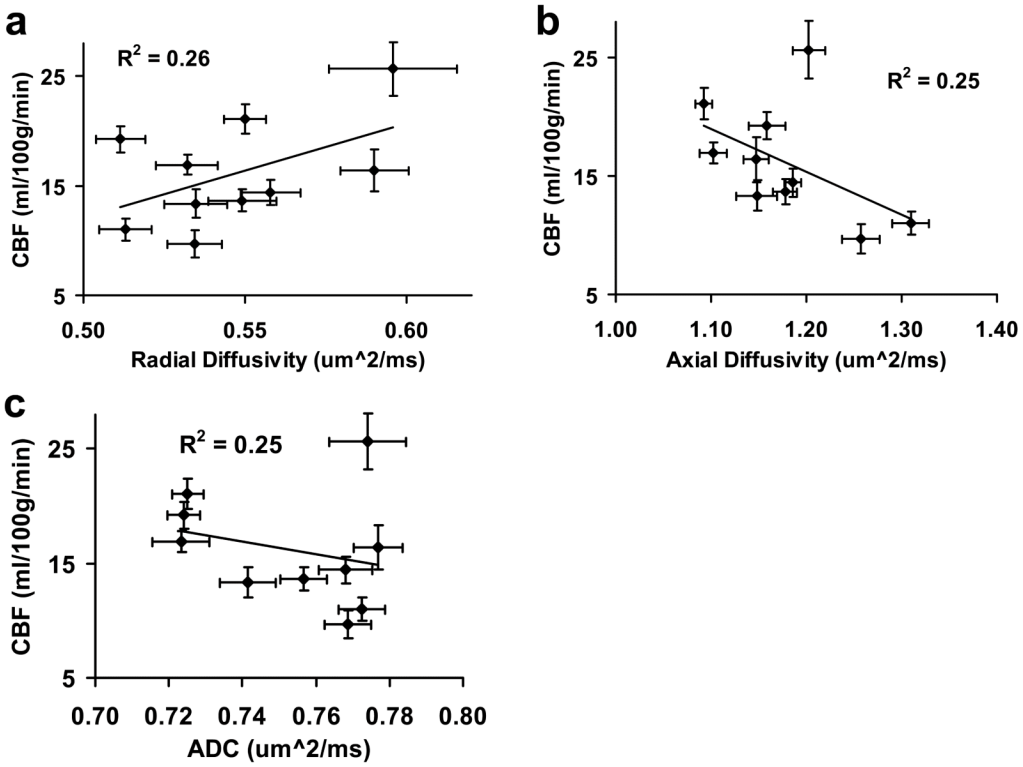

Figure 3.

Scatter plots between CBF and radial diffusivity (a), axial diffusivity (b) and ADC (c). Each symbol represents data from one fiber tract averaged over all subjects. The error bars indicate standard error of mean. CBF was positively correlated with radial diffusivity (P=0.001), but was negatively correlated with axial diffusivity (P=0.003) and ADC (P<0.001).

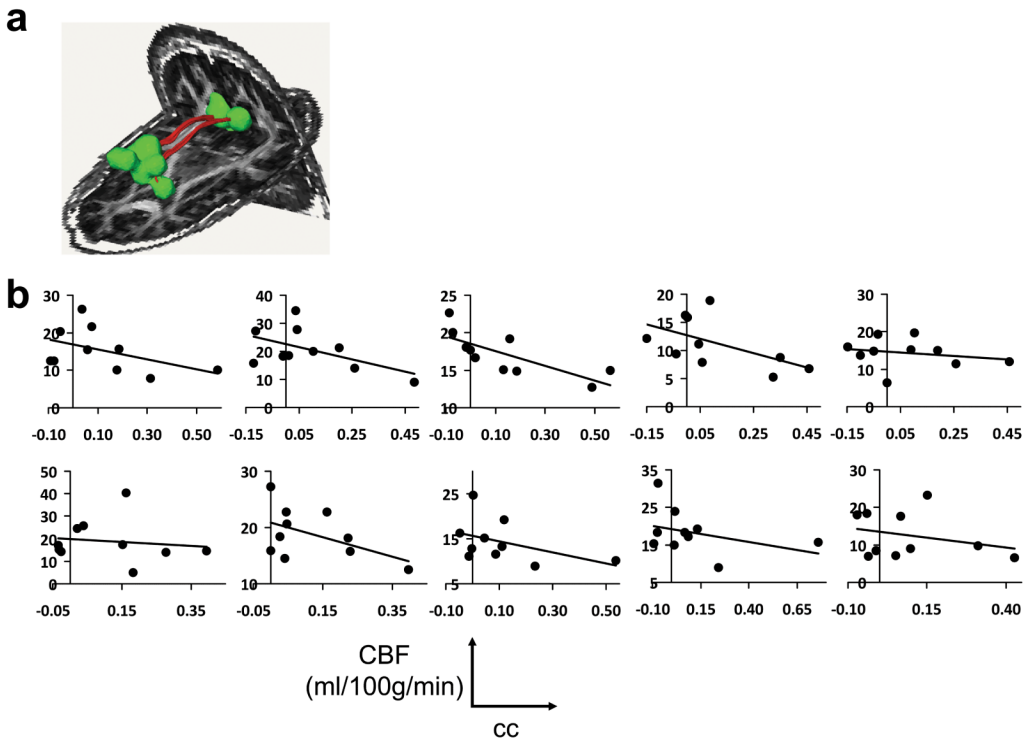

Figure 4.
Relationship between tract-specific CBF and fcMRI cc values. (a) Illustration of "cingulum-in-the-cingulated-cortex" tract and the gray matter nodes in the posterior cingulate cortex and medial frontal cortex. (b) Scatter plots between CBF and fcMRI cc across fiber tracts. Each sub-plot displays data from one subject. Within a sub-plot, different points indicate different tracts. An inverse correlation is observed in all subjects.

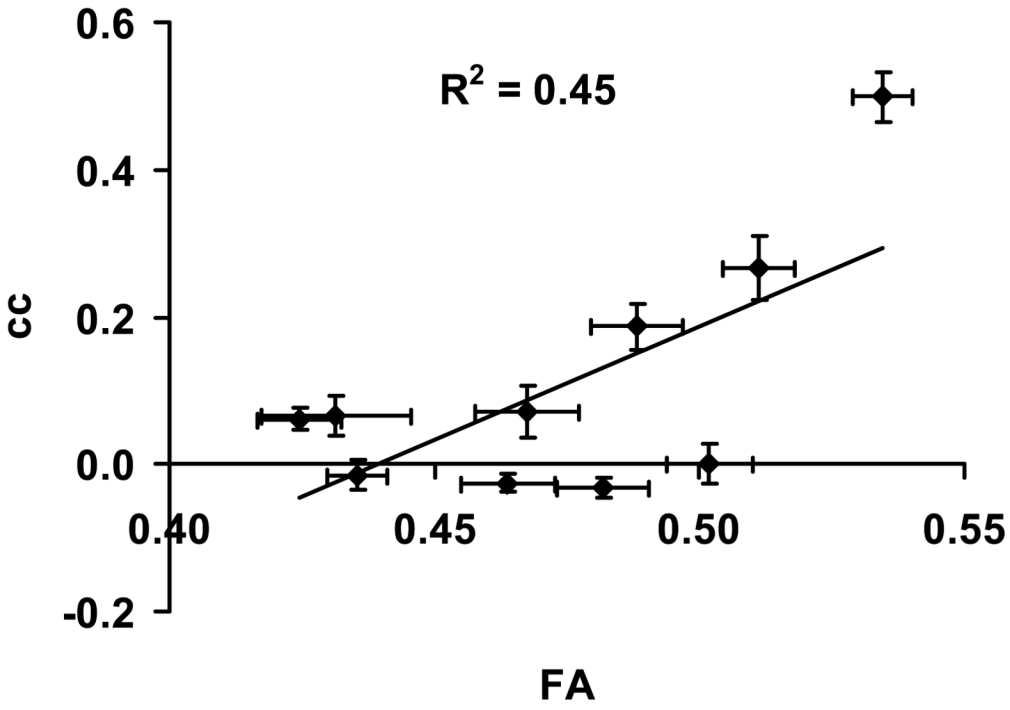

Figure 5.
Scatter plot between FA and fcMRI cc values. Each symbol represents data from one fiber tract (and associated gray matter nodes) averaged over all subjects. The error bars indicate standard error of mean. FA was positively correlated with fcMRI cc ($P<0.001$).

Table 1

Summary of fiber-tract-specific CBF, FA, white matter probability, layer index, SNR of tract-specific CBF as well as the fcMRI cc values from the gray matters that the respective tract connects. The values are listed as mean ± standard deviation (N=10). The fiber tracts are listed in ascending order of CBF. Note that the fcMRI cc values shown here are from the entire ROIs, while the meta-analysis was based on cc values from 10-voxel blocks, in order to account for volume differences across ROIs. The corticospinal tract was excluded from the fcMRI analysis because the terminal of this tract was in the spinal cord which was beyond the spatial coverage of our image acquisition

	CBF (ml/100g/min)	FA (unitless)	White matter probability (%)	Layer index (unitless)	SNR of CBF (unitless)	Correlation Coefficient in fcMRI (unitless)
Forceps Minor of Corpus Callosum	9.7±3.9	0.52±0.02	96.0±0.6	2.96±0.16	4.42±2.21	0.69±0.26
Forceps Major of Corpus Callosum	11.0±3.1	0.56±0.02	91.3±2.4	2.38±0.31	7.51±2.55	0.87±0.06
Cingulum in the Cingulate Cortex	13.4±4.1	0.51±0.02	95.3±1.3	2.44±0.30	6.71±1.80	0.37±0.18
Inferior Fronto-Occipital Fasciculus	13.7±3.3	0.50±0.02	95.0±1.4	3.23±0.94	9.27±2.81	−0.09±0.12
Inferior Longitudinal Fasciculus	14.4±3.7	0.48±0.02	94.1±1.1	2.87±0.17	9.84±3.56	−0.08±0.14
Uncinate Fasciculus	16.4±6.1	0.44±1.2	91.4±1.2	2.09±0.25	7.24±3.59	0.31±0.23
Arcuate Fasciculus	16.9±2.8	0.48±0.03	96.4±1.3	4.44±0.56	10.94±2.96	0.18±0.27
Corticospinal Tract	19.2±3.7	0.51±0.02	95.4±1.2	5.19±0.57	8.84±2.77	-
Anterior Thalamic Radiation	21.1±4.2	0.44±0.01	94.6±0.8	3.41±0.25	14.60±2.75	−0.05±0.26
Cingulum to hippocampus	25.7±7.8	0.47±0.03	90.9±2.1	1.58±0.33	8.33±2.97	0.17±0.23